The Role of Mesoscale Convective Systems in Precipitation in the Tibetan Plateau region

Julia Kukulies[1], Deliang Chen[1], Julia Curio[1]

[1]University of Gothenburg, Department of Earth Sciences, Guldhedsgatan 5c, 413 20 Göteborg
[2]University of Gothenburg, Department of Earth Sciences, Guldhedsgatan 5c, 413 20 Göteborg
[3]University of Gothenburg, Department of Earth Sciences, Guldhedsgatan 5c, 413 20 Göteborg

Key Points:

- Mesoscale convective systems (MCSs) and associated precipitation are tracked in the Tibetan Plateau (TP) region
- Long-lived and large MCSs produce substantial amounts of convective rainfall over the Indo-Gangetic Plain
- Seasonal and extreme precipitation over the TP are dominated by smaller and short-lived convective systems

Corresponding author: Deliang Chen, `deliang@gvc.gu.se`

Abstract

Mesoscale convective systems (MCSs) have been identified as an important source of precipitation in the Tibetan Plateau (TP) region. However, the characteristics and structure of MCS-induced precipitation are not well understood. Infrared satellite imagery has been used for MCS tracking, but cirrus clouds or cold surfaces can cause misclassifications of MCS in mountain regions. We therefore combine brightness temperatures from IR imagery with satellite precipitation data from GPM and track MCSs over the TP, at the boundary of the TP (TPB) and in the surrounding lower-elevation plains (LE) between 2000 and 2019. We show that MCSs are less frequent over the TP than earlier studies have suggested and most MCSs over land occur over the Indo-Gangetic Plain (LE) and the south of the Himalayas (TPB). In the LE and TPB, MCSs have produced 10 % to 55 % of the total summer precipitation (10 % to 70% of summer extreme precipitation), whereas MCSs over the TP account for only 1 % to 10 % to the total summer precipitation (1 % to 30 % of the total summer extreme precipitation). Our results also show that MCSs that produce the largest amounts of convective precipitation are characterized by longevity and large extents rather than by high intensities. These are mainly located south of the TP, whereas smaller-scale convection makes a greater contribution to total and total extreme precipitation over the TP. These results highlight the importance of convective scale modeling to improve our understanding of precipitation dynamics over the TP.

Plain Language Summary

Storm systems that extend over several hundred kilometers can produce substantial rainfall amounts over short periods. They are a risk for people's life and livelihoods, as they may lead to flooding, extreme winds and heavy rainfall. The Tibetan Plateau (TP) has gotten increasing attention because it experiences drastic changes in the water cycle as a response to global warming. Although it is known that large storm systems develop over the TP and in its populous surrounding regions, the rainfall characteristics from these storms are not well researched. It is not trivial to identify storm systems in satellite images over high mountain regions, because high clouds and cold surface temperatures can give signals similar to those of storm clouds. We use therefore a new method to track large storm systems in satellite images over the TP, in order to clarify their role in the water cycle and extreme rainfall. Our results show that the storms that produce most heavy rainfall occur over the Indo-Gangetic Plain and south of the Himalayas. Storm systems over the TP are generally much smaller in size and shorter in duration, which means that climate model simulations at high spatial resolutions are needed to further investigate these.

1 Introduction

Mesoscale convective systems (MCSs) are organized convective storm complexes, which extend over several hundreds of kilometers and produce large areas of convective and stratiform precipitation (Houze, 2004). MCSs have more complex dynamics than unicellular convective storms, but are primarily defined by their spatial extent (Houze, 2004). Many different forcings can drive mesoscale organization of convection. Thus, the structure and precipitation characteristics of an MCS can take different forms depending on the region of genesis. Weather systems that are usually classified as MCSs include tropical cyclones, squall lines, lake-effect snow events and polar lows. In the continental midlatitudes, MCS formation is often related to mountain flow dynamics and MCSs are often found in or close to mountain regions. On the leeside of the Rocky Mountains (over the Great Plains) (Hitchcock et al., 2019; Cheeks et al., 2020; H. Hu et al., 2020), in the West-African Sahel (Redelsperger et al., 2002; Vondou et al., 2010; Klein et al.,

2018) and in the European Alps (Morel & Senesi, 2002; Feidas, 2017), MCSs produce a significant portion of the total precipitation in a season and can lead to severe weather.

The Tibetan Plateau (TP) covers an area of two and a half million square kilometers and is the world's most extensive mountain region. The headwaters of most of Asia's major rivers rise in the mountains of the TP, and their discharge regimes are mainly dominated by monsoonal precipitation (Zhang et al., 2013). An outstanding characteristics of the TP is its high elevation and steep topography, which results in complex interactions between local mountain features and large-scale atmospheric dynamics. Studies have identified MCSs to be one of the most important precipitation-producing mechanisms over the TP (Tao & Ding, 1981; B. Wang, 1987; Li et al., 2008; Sugimoto & Ueno, 2012). Some extreme rainfall and flood events in the populated downstream regions to the south and east of the TP have been attributed to MCSs and to mesoscale vortices that formed over TP (Yasunari & Miwa, 2006; Shi et al., 2008; Xiang et al., 2013; Rasmussen & Houze Jr, 2012). This demonstrates that MCSs can pose a direct threat to life, to people's livelihoods, to crop yields and to infrastructure. In addition, MCSs play an important role in the hydrological cycle, as they may account for a significant amount of the annual or seasonal rainfall, for example in North America (Fritsch et al., 1986). Convection-permitting model simulations project increases in MCS intensity for some regions of the globe (Prein, Liu, Ikeda, Trier, et al., 2017; Fitzpatrick et al., 2020) and convective precipitation is likely to increase at much larger rates than the average precipitation increase by 7 % per degree of warming according to the Clausius-Clapeyron relation (Berg et al., 2013; Ban et al., 2015). It is therefore crucial that we understand the scales and formation processes for extreme convective precipitation, particularly for mountain regions like the TP, which are likely to experience drastic environmental changes due to global warming (Bibi et al., 2018; Yao et al., 2019).

Despite the fact that much literature on convection in the TP region focuses on MCSs, the main drivers behind the systems and their significance for current and future precipitation regimes are not well understood. It is not clear how characteristics of MCSs that initiate over the TP differ from those of the monsoon-related convective systems that occur south of the Himalayas (Houze et al., 2007; Romatschke et al., 2010; G. Chen & Kirtman, 2018). A number of studies that researched MCS at elevations higher than 3000 m above sea level (a.s.l.) have identified the central and eastern parts of the TP as the main source regions for MCS genesis (Jiang & Fan, 2002; Li et al., 2008; Sugimoto & Ueno, 2012; L. Hu et al., 2017). However, due to the difficulty in attributing precipitation events to specific storm systems, the role of MCSs in precipitation could only roughly be estimated. In addition, convective cells can be misclassified when infrared (IR) satellite imagery is used to track MCSs in a high mountain region and image scenes include cold cirrus cloud tops (Rossow & Schiffer, 1999; L. Hu et al., 2017) or cold surfaces under clear-sky conditions that result in a similar IR brightness temperature (Esmaili et al., 2016). Observation-based studies of MCSs are therefore more limited than model studies for the TP region and most cover only a few years, because high-resolution satellite records of more than decade's length have only recently become available. It is crucial that we establish an accurate climatology of MCSs and understand their role in precipitation so that we can advance our knowledge about precipitation dynamics in the TP region. The effect of MCSs on precipitation is key to an improved understanding of the drivers and scales for extreme precipitation which in turn is necessary for more accurate estimations of future changes to precipitation regimes and extreme events.

The aim of this study is to describe the characteristics of MCSs in the TP region using a novel tracking method to interpret satellite observations covering the past two decades (from 2000 to 2019). To provide a broad overview of different types of MCSs, we compare MCSs over the TP with MCSs that cross the TP boundary (TPB) and MCSs that develop over the surrounding lower-elevation (LE) regions. We focus on the structure and characteristics of MCS-induced precipitation and the contribution of MCSs to seasonal and extreme rainfall.

The manuscript is organized as follows. In section 2, we describe the tracking algorithm and datasets used in this study and also summarize results from a pilot study in which we tested the sensitivity of the tracking to different thresholds and criteria. In section 3, we present the results including the spatial and temporal characteristics of MCS tracks and the precipitation features associated with them. The role of MCSs for precipitation in the TP region and some possible mechanisms for MCS formation are discussed in section 4. Finally, a summary and the main conclusions are given in section 5.

2 Data and Methods

2.1 Tracking algorithm

One of the most commonly used methods to identify MCSs is to detect a contiguous area of cloud top temperature minima in IR satellite imagery. A specific type of MCS is a so-called *Mesoscale convective complex* (MCC), originally defined by Maddox (1980). MCC is a cloud system with a continuous area of at least 100 000 km^2, within which the maximum temperature is -32°C (241 K) and which includes a region of at least 50 000 km^2, within which the maximum temperature is -52°C (221 K). An additional criterion is that these two conditions must persist for at least six hours for a MCC to be identified. A myriad of studies has followed an approach similar to this for global and regional MCS tracking, mostly using cloud top temperature thresholds of between 230 K and 255 K over minimum areas that range from 2000 km^2 to 50 000 km^2 (Sugimoto & Ueno, 2012; Esmaili et al., 2016; G. Chen & Kirtman, 2018; Klein et al., 2018; Cheeks et al., 2020). Most observational MCS studies in the TP region have used global databases for tracking (Li et al., 2008) or thresholds that are also used in global analyses for MCS identification (Guo et al., 2006). However, using universal thresholds can be problematic in a mountain environment like the TP and can lead to low surface temperatures from high mountain tops being confused with high cloud tops from deep convective clusters, particularly at night and during the winter. This has, for example, been discussed in Esmaili et al. (2016), who presented a global cloud cluster tracking with unrealistically high amounts of cloud clusters over the TP during winter. The atmospheric transmittance at wavelengths corresponding to the IR channels used for tracking ($\sim$ 10.8 μm) is relatively high, while surface emissivity at these wavelengths is generally low for dry regions (Schädlich et al., 2001). This means that retrieved clear-sky brightness temperatures are lower than the actual surface temperatures and that there is an additional risk to confuse cold surfaces with high cloud tops. Another risk of exclusively using cloud top temperatures as a proxy for convective activity in mountain regions is that convective systems can also be confused with cirrus cloud shields that are not necessarily the remnants of a storm system. Kukulies et al. (2019) showed that cirrus clouds are among the most frequent cloud types over the central and southern parts of the TP between May and September. To address the above named issues, we have thus used a new objective tracking method that reduces misclassifications of MCS attributable to cirrus cloud layers and cold surfaces.

We use half-hourly satellite precipitation estimates from the Global Precipitation Measurement Mission (GPM) in combination with brightness temperatures from IR imagery. The brightness temperatures used in this study are from merged, angle-corrected IR observations acquired by sensors on board Meteosat, GMS/Himawari, Meteosat and GOES. The NCEP/CPC (National Centers for Environmental Prediction/Climate Prediction Center) dataset can be downloaded from NASA GES DISC (`https://disc.gsfc.nasa.gov/datasets/GPM\_MERGIR\_V1/summary`) at 30 minute resolution and with 4km grid spacing. In order to obtain the same spatial resolution as the satellite precipitation

Table 1. Criteria for different tracking methods

Test	Threshold	Minimum Extent	Time Requirement
T_b	<= 230 K	100 grid cells	>= 6 hrs
T_b *cold core*	<= 230 K	100 grid cells	>= 6 hrs
	< 200 K	1 grid cell	1/lifetime
T_b *heavy rain core*	<= 230 K	100 grid cells	>= 6 hrs
	< 200 K	1 grid cell	1/lifetime
	>= 5 mm h^{-1}	10 grid cells	1/lifetime
Precip	>= 5 mm h^{-1}	10 grid cells	>= 6 hrs
TCS	<= 230 K	20 grid cells	>= 3 hrs
	< 200 K	1 grid cell	1/lifetime
	>= 5 mm h^{-1}	5 grid cells	1/lifetime

**The detection and tracking criteria are modified from Yuan and Houze Jr (2010) and G. Chen and Kirtman (2018)*

data product GPM IMERG V06 (`https://disc.gsfc.nasa.gov/datasets/GPM_3IMERGHH_06/summary?keywords=GPM\%20IMERG\%20v06\%2030\%20MIN`), which has a spatial resolution of 0.1 °, we regridded the brightness temperature data to match this. The tracking was performed in 30 minute time steps to match the original temporal resolution of both datasets, for the period 2000 to 2019.

The main difference between our tracking method and more conventional tracking methods is that we use lower temperature thresholds and require that cloud cells develop a cold core that drops below 200K at least once during their lifetime and that at least 10 % of the minimum cloud area (10 pixels) correspond to a rain rate of at least 5 mm h^{-1}. The purpose of these extra criteria is to avoid high cirrus clouds or stratiform cloud layers with lower rain rates being mistakenly identified as MCSs. By combining IR and precipitation, we increase the captured lifetime of the evolving cloud cells (more details are given in the following section).

Using the python package *tobac* (Heikenfeld et al., 2019), cloud features are identified at each time step using Gaussian filtered brightness temperatures (T_b) and then linked over time based on their location and propagation speed. More details about this linking method can be found in Heikenfeld et al. (2019). We define a cloud feature as a contiguous area of at least 100 pixels (about 10 000 km^2) in which brightness temperatures do not exceed 230 K (Table 1). With this minimum area threshold we focus on MCS at the upper bounds of the *mesoscale* (Orlanski, 1975), because we assume that these are the MCS with the largest impacts and the MCS which are more likely to interact with the large-scale atmospheric circulation. Additionally, previous studies have identified mesoscale vortices with horizontal dimensions between 100 - 1000 km over the TP (B. Wang, 1987; Tao & Ding, 1981; Yasunari & Miwa, 2006), so this study allows us to check whether cloud cells over the TP can develop at these scales. Each detected cloud feature is then augmented by including adjacent pixels with brightness temperatures up to 245 K (235 K for December, January and February). This allows us to in-

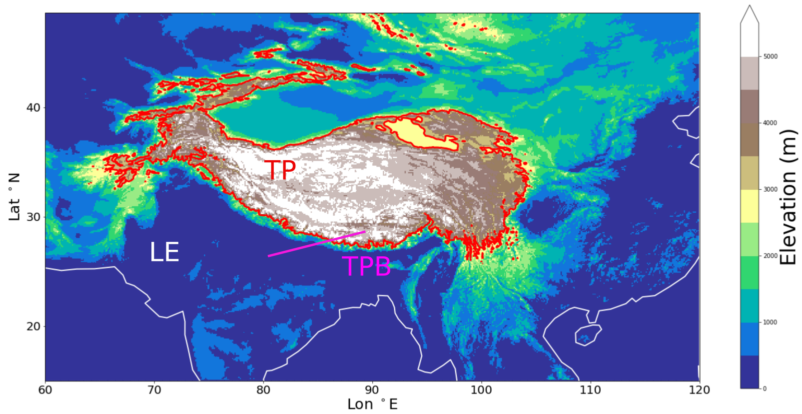

Figure 1. Study area (15 – 50 °N, 60 – 120 °E) for regional MCS tracking. The colors show elevations [m a.s.l.] and the red line indicates the 3000 m boundary of the TP. MCS are divided into systems located outside of this boundary (LE), systems over the TP and systems, which cross the 3000 m boundary during their lifetime (TPB).

clude as much of the cloud cell as possible, while excluding surrounding cold surfaces. The thresholds for selecting additional pixels to augment detected cloud features were chosen by evaluating distributions of hourly surface temperatures from ERA5 (`https://cds.climate.copernicus.eu/cdsapp#!/dataset/reanalysis-era5-single-levels?tab=overview`) and by performing test runs with different thresholds. Figure 2 shows that our cloud top temperature threshold of 245 K (235 K during winter), it can be does not overlap with the corresponding seasonal distribution of hourly surface temperatures. Once cloud features have been detected and augmented for each time step, they are linked over time and a cloud system must persist for at least 6 hours to be retained as a potential MCS. Due to computational resources linking of features was performed on yearly aggregated files, which means that MCS at the boundary between two years appear as separate tracks. Finally, two additional criteria are applied. To be classified as an MCS, the feature must have an area of at least one pixels where the maximum temperature does not exceed 200 K and an area of at least 10 pixels ($\tilde{1}$0 % of minimum cloud area) with rain rates of at least 5 mm h^{-1} at least once during their lifetime (T_b *heavy rain core* in Table 1).

It should be noted that the study area (15 – 50 ° N, 60 – 120 °E) encompasses regions with substantially different precipitation regimes, such as the Indo-Gangetic Plain, which are dominated by monsoon depressions (Hurley & Boos, 2015) and the generally drier TP (Fig. 1). Considering such a wide area with diversified background climates provides a regional overview of MCSs, allowing those over the TP to be compared with those initiated over more populous regions. In this study, we distinguish between three classes of systems: MCSs and precipitation events that remain within the 3000 m boundary of the plateau (TP), MCS that cross the 3000 m boundary with at least 10 pixels once during their lifetime (TPB) and MCSs and precipitation events outside the 3000 m boundary at lower elevations (LE). These three subregions are visualized in Figure 1.

Figure 3 shows brightness temperatures and precipitation data for the study area. The snapshot shows a mature MCS on July 20th, 2008 and the succeeding plots show the evolution of the MCS track. The black line indicates the center of the MCS for ear-

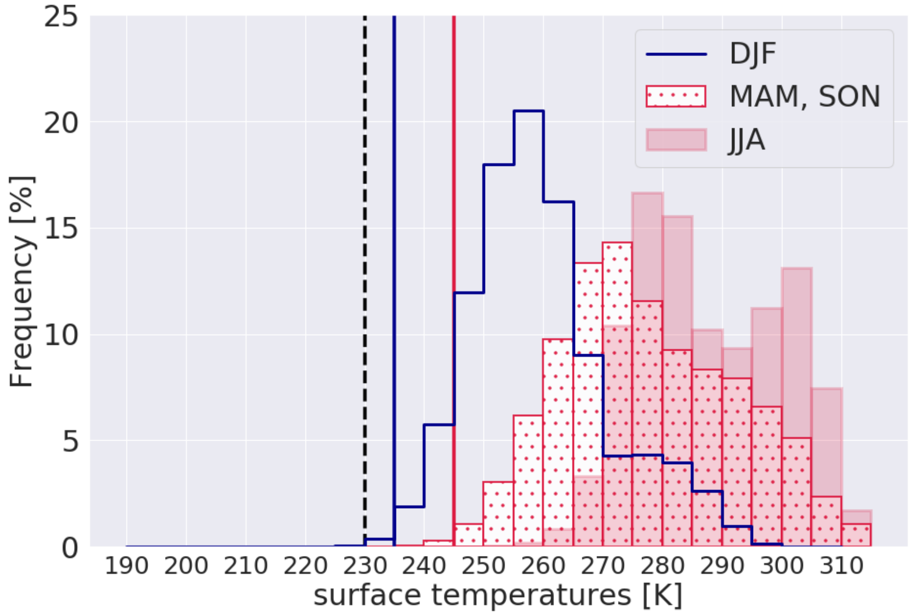

Figure 2. Seasonal distributions of hourly surface temperature over the TP (for surface elevations >= 3000 m) based on ERA5 data for 2000 to 2019. The dashed black line shows the threshold used for detection of cloud features and the vertical red and blue lines indicates show the thresholds used to select pixels for augmentation of cloud features in winter (December to February) and outside of the winter season (March to November), respectively.

lier time steps and the red dot indicates the center of the MCS at the time of the snapshot. This tracked MCS produced substantial amounts of heavy rainfall in the downstream region to the east of the TP. We use this well-known event, which also coincided with a mesoscale disturbance in vorticity (Curio et al., 2019), as a case study to prove that our tracking algorithm is able to capture the known evolution of the system.

2.2 Comparison of tracking methods

It should be noted that the atmospheric variable selected as a proxy for convection (e.g. cloud top temperature, precipitation, vorticity, wind speed) determines the spatial and temporal characteristics of the tracked MCS. There are many advantages to using precipitation, as it is a key component in the water cycle that has direct impacts on hydrology and society. It is also reasonable straightforward to compare precipitation tracks with model and reanalysis data, whereas cloud top temperatures are usually not available as standard products. However, the part of an MCS in which precipitation is produced is usually smaller and more short-lived than the cloud system as a whole. Hence, using precipitation as a proxy for convection provides a more limited view of both the structure and evolution of tracked storm systems compared to cloud top temperature. This motivated us to perform a pilot study, in which we compare four algorithms with different tracking criteria to improve our understanding of the implications of different tracking methods for MCSs in the TP region.

Table 1 summarizes the criteria for the four different algorithms. First, we performed tracking using only brightness temperatures (T_b) applying the same criteria to these as we used in our combined tracking for cloud feature identification. We then added the cold core criterion (in *T_b cold core*) and the heavy rain criterion (in *T_b heavy rain core*) from our combined tracking (described in section 2.1). Finally, we implemented tracking based on areas of contiguous precipitation using different rain rate thresholds. The results for the run with a threshold of 5 mm h^{-1} are presented here, because it represents the best compromise for which precipitation cells could be tracked in the more humid parts of the study domain as well as over the drier TP. In addition, this threshold lies within the range of rainfall intensities that are typically used to classify convective precipitation (Gaál et al., 2014) and has also been used by other MCS studies (Prein, Liu, Ikeda, Bullock, et al., 2017).

For comparison, we also implemented tracking for convective systems within the TP (elevation is equal or above 3000 a.s.l.), using lower minimum thresholds for area ($>=$ 20 pixels) and persistence ($>=$ 3 hours) (*TCS* in Table 1). These smaller and more short-lived systems correspond to the meso-β scale (20 to 200km) according to the definition in Orlanski (1975), whereas the tracking methods described in the previous paragraphs were designed to identify larger and longer-lived MCS at the meso-α scale (200 to 2000km). We applied the same cold core and heavy rain criteria to this meso-β tracking method as for the meso-α tracking methods (Table 1) and found that reducing the size requirement for the heavy rainfall area did not result in more systems being identified (figure not shown). All systems identified sing the *TCS* tracking method developed a heavy rain core once during their lifetime with precipitation of at least 5 mm h^{-1} over an area of at least 5 grid cells and of at least 3 mm h^{-1} over at least 10 grid cells. The purpose of these additional runs is to investigate the role of convective cells at the lower bounds of the mesoscale over the TP. Due to limited computer capacity, the meso-β tracking could not be implemented for the entire study area as it would result in too many cloud feature combinations that would have to be assessed to determine linkages across time steps.

Figure 4 shows the main characteristics of MCSs identified by the four different tracking methods (*T_b, T_bc cold core, T_b heavy rain core, Precip*). The diurnal cycle for features tracked using precipitation (*Precip*) has a bimodal distribution (Fig. 4a), whereas the other tracking runs are marked by a clear evening peak. The different diurnal curves

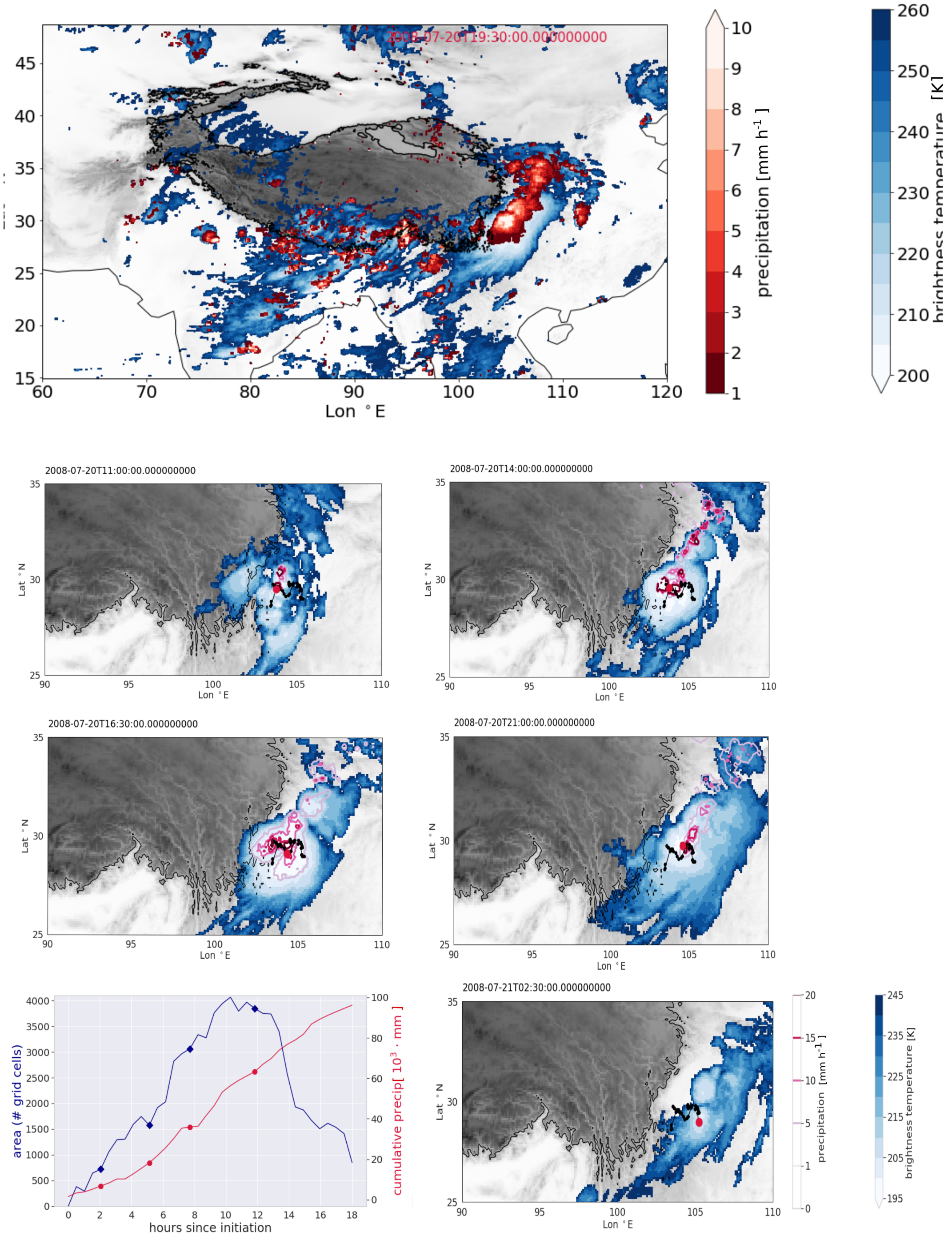

Figure 3. Example of a tracked MCS at the eastern boundary of the TP in July, 2008. The upper panel shows a snapshot of half-hourly brightness temperatures with GPM IMERG precipitation. The evolution of the tracked cloud cell and of the corresponding precipitation feature are shown in the lower panels, where the black line indicates the MCS center at the preceding and succeeding time steps and the red dot marks the center in the imaged time step. The zoomed images correspond to the time steps indicated by markers in the timeseries graph for cloud area and accumulated precipitation.

can be explained by the fact that *Precip* only contains the MCS features when it is raining, while the other tracking methods capture the evolution of the MCSs more completely, including non-precipitating hours.

The T_b tracking identified a significantly higher numbers of TPB systems during winter (Fig. 4b) and generally detected more TPB systems than LE systems (Fig. 2). A similar result was found by L. Hu et al. (2017), who used MCS data from the global *ISCCP Convective Tracking Database* (C. Wang et al., 2018). By filtering with a threshold for optical depth, they found that the winter maximum for MCS events changed to a summer maximum. This is consistent with the well established understanding of summer convection over the TP (Flohn & Reiter, 1968; Ye & Wu, 1998) and confirms the impact of MCS misclassification on climatologies, due to cold surfaces or cirrus clouds, that was discussed earlier.

When identified and tracked using precipitation only (*Precip*), MCSs were perceived to exhibit shorter lifetimes (Fig. 4c) and a reduced extent, which barely overlap with the MCS area distributions derived from the other three tracking methods (Fig. 4d). This is due to the fact that the precipitating area covers only a part of the cloud system, which often seems to be confined to the area with the coldest cloud top temperatures (Fig. 3). On top of that, precipitation is not necessarily contiguous in time and space, but can occur in a more scattered manner when MCS are weakened and re-initiated. This also explains the higher number of systems from *Precip* compared to T_b, T_b*c cold core* and T_b *heavy rain core* (Table 2). As mentioned earlier, a further advantage of the combined brightness temperature-precipitation tracking (T_b *heavy rain core*) is, that it can capture both a larger portion of the cloud cell evolution as well as the evolution of the precipitating area of a cloud system.

As described in section 2.1, the number of TPB tracks in Table 2 contain both systems which only partly cross the 3000 m boundary and systems which are entirely within the TP. Of these MCS tracks, the total number of MCSs that formed (or were first detected) over the TP was only 58 (around 4 MCSs per year). In contrast, tracking smaller-scale convective systems (*TCS*) over the TP resulted in identification of a total of 1428 cases (around 75 cases per year). The additional systems that were identified and tracked using the *TCS* method shows the relative prevalence of smaller-scale convective systems over the TP.

2.3 Analysis of MCS and associated precipitation features

Since the python package *tobac* allows for feature tracking using multiple thresholds, each identified cloud feature is assigned to an intensity category. The intensity categories are defined as areas within the detected cloud feature where a specific brightness temperature threshold is exceeded (between 195 K and 230 K). We use the cloud feature characteristics at each time step (shape, area, brightness temperature intensity, precipitation features) and the characteristics of the track that describes the MCS evolution (lifetime, total precipitation, propagation speed, propagation direction) to compare different MCS types. Firstly, all tracked MCSs in the study area (Fig. 3) were assigned to one of the four classes based on their propagation direction (northward and eastward) and location (denoted as TPB east, TPB north, LE east and LE north). These two propagation directions were chosen, because most of the detected MCS trajectories follow one of these directions, which match the directions of major large-scale atmospheric circulation systems that affect the region (e.g. mid-latitude westerlies and the northward propagating Indian summer monsoon). The total amount of eastward-moving TPB systems were slightly higher than for LE features, but the northward-moving LE systems exceeded the number of northward-moving TPB systems.

To investigate the importance of MCS for precipitation from a climatological perspective, the total amount of precipitation is calculated for each of the detected cloud

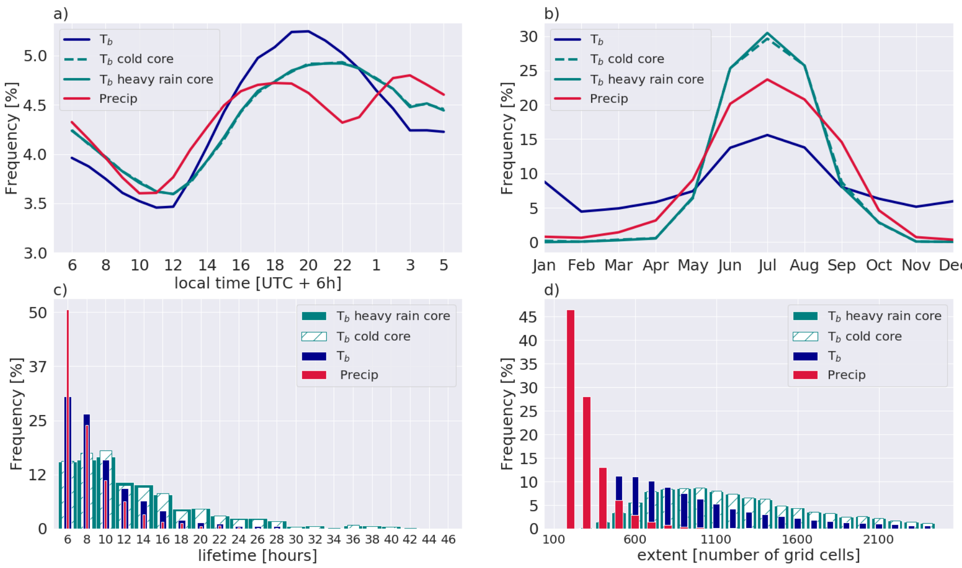

Figure 4. Comparison of characteristics for MCSs identified using four different tracking methods. The subfigures show the a) average diurnal cycle for the frequency with which a feature was identified within the entire study area b) average seasonal distribution for features identified over the TP c) distribution of the lifetime [h] for all MCS tracks and d) distribution of the extent [number of grid cells] of all tracked MCS features.

Table 2. Total number of MCS between 2000 and 2019 using different tracking methods.

MCS type	Tracking method	number of tracks (average per year)
LE	*Precip*	5465
TPB	*Precip*	4090
total	*Precip*	**9555**
LE	T_b	563
TPB	T_b	3117
total	T_b	**3680**
LE	T_b *cold core*	294
TPB	T_b *cold core*	261
total	T_b *cold core*	**555**
LE	T_b *heavy rain core*	277
TPB	T_b *heavy rain core*	240
total	T_b *heavy rain core*	**517**
TP	*TCS*	75

features and compared to total monthly and seasonal precipitation received at every grid cell. Other precipitation mechanisms than MCSs may dominate the total annual and seasonal precipitation, and so we also examine the importance of MCS-associated rainfall only for extreme precipitation events. The same reasons that were given for the choice of the rain rate threshold in the heavy rain core of an MCS (see section 2.2), motivated us to define extreme convective precipitation as all precipitation that falls at rain rates equal to or higher than 5 mm h^{-1}.

3 Results

3.1 Spatial and temporal characteristics

Figure 5 shows histograms of the seasonal occurrence (a), mean propagation speed (b), lifetime (c) and mean extent (d) for LE north, LE east, TPB north and TPB east. The seasonal cycles for TPB systems have a distinct peak in June (Fig. 5a), which is directly follows the onset of the Indian summer monsoon season over the TP. Both LE east and LE north also exhibit an early summer peak of MCS occurrences, which is, however, much more pronounced than MCSs in the TPB region. While more than 75 % of TPB east and TPB north occur between June and October, the frequency of MCSs that occur in LE north and LE east is significantly smaller during autumn and drops by around 10 % from the month of September.

The distributions of mean propagation speed, lifetime and mean extent are similar for the four MCS types LE north, LE east, TPB north and TPB east (Fig. 5b-d), showing that MCS in each subgroup still exhibit a large variety of characteristics that are not primarily affected by their propagation direction (mean environmental wind) and elevation. More than half of the tracked MCS in each subgroup do not last longer than 12 hours, but all four MCS types include examples of long-lived MCS that last longer than 30 hours (Fig. 5c). The distribution of MCS extent is right-skewed, similar to the distribution of MCS lifetime, and MCSs with the greatest extent are slightly more frequent for LE north and LE east types than for TPB east and TPB north types (Fig. 5d). Most of the tracked MCSs have a mean extent between 1000 and 1500 grid cells, which corresponds to an area of about 100 000 – 150 000 km^2. This shows that the area of the cloud shield for most of the systems is at least 10 times as large as the required minimum cold area (Fig. 5d) and that the horizontal dimensions of of the dominating MCSs type in the study area are comparable to *Mesoscale Convective Clusters* (described in section 2).

It can be seen clearly in Figure 6 that the Indian subcontinent and adjacent ocean are the regions, where most of the MCSs originate. The Indo-Gangetic Plain and the Himalayas are the initiation location for TPB systems, rather than the TP itself (Fig. 6a-b). The few MCSs that initiate (or first detected) over the TP mainly form over the eastern parts of the TP and are, except for a few cases, transported eastward (Fig. 6a). MCSs that are transported towards the TP and are therefore included in the TPB class may have travelled large distances, but they do not reach far behind the Himalaya mountain ranges, but stop south of the Himalayas, where most of the TP rainfall occurs (Kukulies et al., 2020).

To compare MCSs over the TP with systems in the surrounding regions, we selected TPB systems that formed over the TP and either remained within the boundary of the TP or moved out of the TP. Figure 3.1a) shows the location of the centers of these systems at the time of initiation (when they first tracked as a cloud feature), when they reach maturity (the age of a cloud feature when its embedded area of precipitation with at least 5 mm h^{-1} is greatest) and when they dissipate (the last time of they area tracked as a cloud feature). It is important to understand the diurnal evolution of MCSs that originate over the TP, because they may be closely linked to topographically-driven diur-

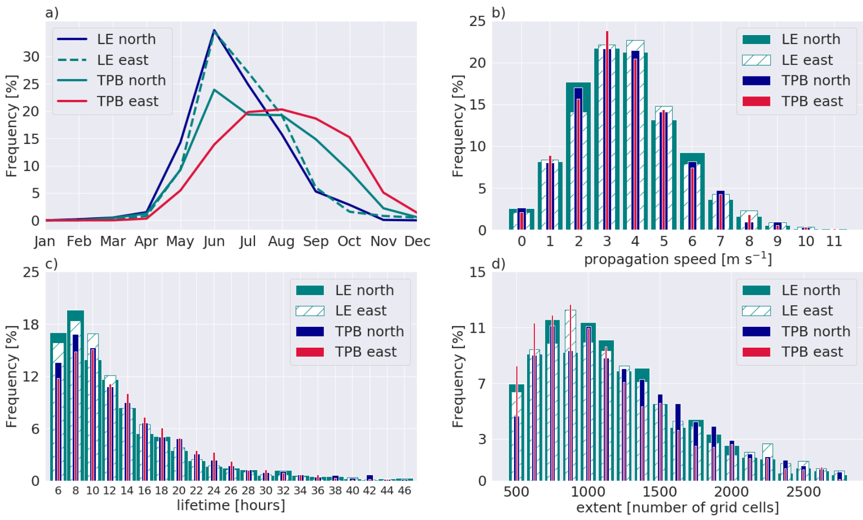

Figure 5. Spatial and temporal characteristics of northward- and eastward-moving MCSs in the LE and TPB regions. The histograms show the relative frequencies [%] for a) seasonal occurrence [%], b) mean propagation speed [m^{-s}], c) lifetime [h] and d) mean extent [number of grid cells].

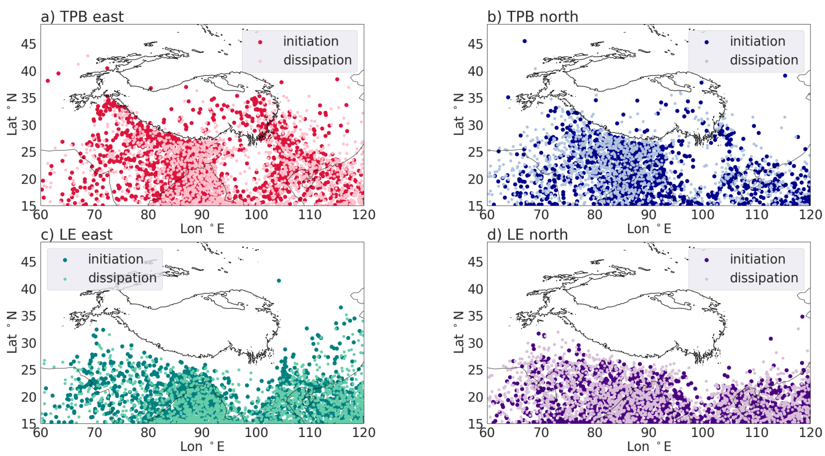

Figure 6. Location of MCS centers at the time of initiation and dissipation for a) TPB east, b) TPB north, c) LE east and d) LE north. Markers depict the mean longitude and latitude for detected cloud features at initiation (the time step at which it is first detected) and dissipation (the last time step in which the feature is detected).

nal flow patterns. Figure 3.1b) suggests that MCSs follow a common pattern of diurnal evolution over the TP, with initiation around noon (12:00 LST), maturity and dissipation occurring late night or in the early morning (between 00:00 and 5:00 LST). The resulting evening and night peaks in precipitation are consistent with the general diurnal cycle of precipitation over the TP (Kukulies et al., 2019) and indicates that the diurnal flow is an important component for the organization of convective cells into larger systems.

3.2 Precipitation characteristics

3.2.1 Contribution to total and extreme precipitation

Figure 8 shows seasonal contributions of precipitation from tracked MCS cloud features to the total precipitation and to the total extreme precipitation (where extreme precipitation is from rainfall events with a rate of at least 5 mm h^{-1}). During spring, the highest MCS contribution to rainfall is over the ocean (Bay of Bengal), and the spatial pattern of the contribution is similar for both total and total extreme precipitation (Fig. 8a-b). Locally, rainfall from MCSs accounts for up to 30 % of the total rainfall over land, but less than 1% of the precipitation iver the TP (Fig. 8a-b). Between June and August, the contribution of MCSs to both total and total extreme precipitation increases substantially (Fig. 8c-d). Although the MCS contributions to precipitation over the TP are significantly lower lower than the contributions for the surrounding regions, the contributions to extreme precipitation are between 30 and 70 % to the south of the Himalayas and over the Indo-Gangetic Plain. The largest contributions over the TP are in the eastern part of the TP, where MCS precipitation accounts for up to 30 % of the seasonal local rainfall. MCS precipitation contributes significantly to the seasonal rainfall over land outside the TP (Fig. 8c-d), and there are only few local maxima over the ocean and at the coast in India for the contribution in winter (Fig. 8g-h).

These results confirm our hypothesis that organization of convective systems, which contribute to total summer precipitation and extreme rainfall over the TP occurs on a smaller scale here than in the surrounding regions, where MCSs provide a large portion of both the total extreme rainfall and the total summer rainfall. In comparison, the systems tracked over the TP (TCS) using a smaller area threshold (see section 2.2 and Table 1) make a significantly higher contribution to precipitation locally during the summer months (Fig. 9). In contrast to the June peak of MCSs for TPB east and TPB north, most of the identified smaller-scale convective systems over the TP occurred between July and August. These systems account for between 25 and 35 % of the total monthly rainfall over large areas of the central and eastern TP. We also see a strong difference between the contribution of these systems to total and to total extreme precipitation. The contributions to extreme precipitation have strong local maxima and therefore a patchy spatial pattern with many grid cells for which more than 50 % of local extreme precipitation is accounted for by tracked systems. A large area of high values for the contribution occurs at the eastern edge of the TP (Fig. 9). This region is the same region that had the highest values MCS contributions over the TP (Fig. 8). There is no clear pattern linking the contribution to precipitation with topography, but it should be noted that small-scale convective systems contribute to summer precipitation even at elevations greater than 5000 m a.s.l. (Fig. 9). This means that organization of convection over a few 10^1 km is not confined to the lower elevations over the TP.

3.2.2 Convective precipitation

The snapshot in Figure 3 is a typical example of an MCS, and shows that the convective core with heavy precipitation is often surrounded by a larger area of stratiform precipitation at moderate rain rates and by an even larger area of non-precipitating clouds. Although these stratiform cloud shields may extent over a greater area, the convective

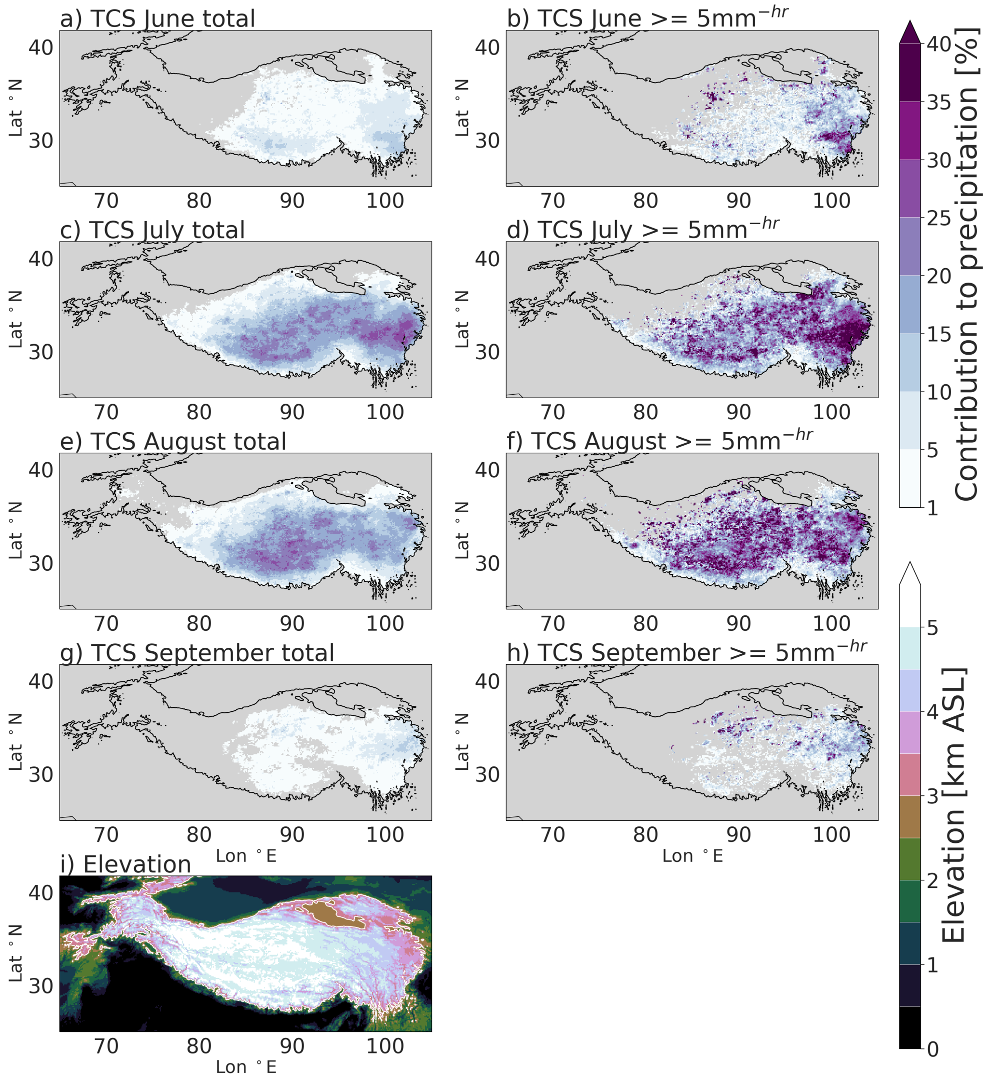

Figure 7. Spatial and temporal evolution of MCSs that initiated over the TP between 2000 and 2019 (58 cases). The left panel (a) shows locations for the MCS centers at initiation, maturity (time associated with maximum precipitation) and dissipation. The right panel (b) shows the average time of the day for initiation, maturity and dissipitation of MCSs over the TP.

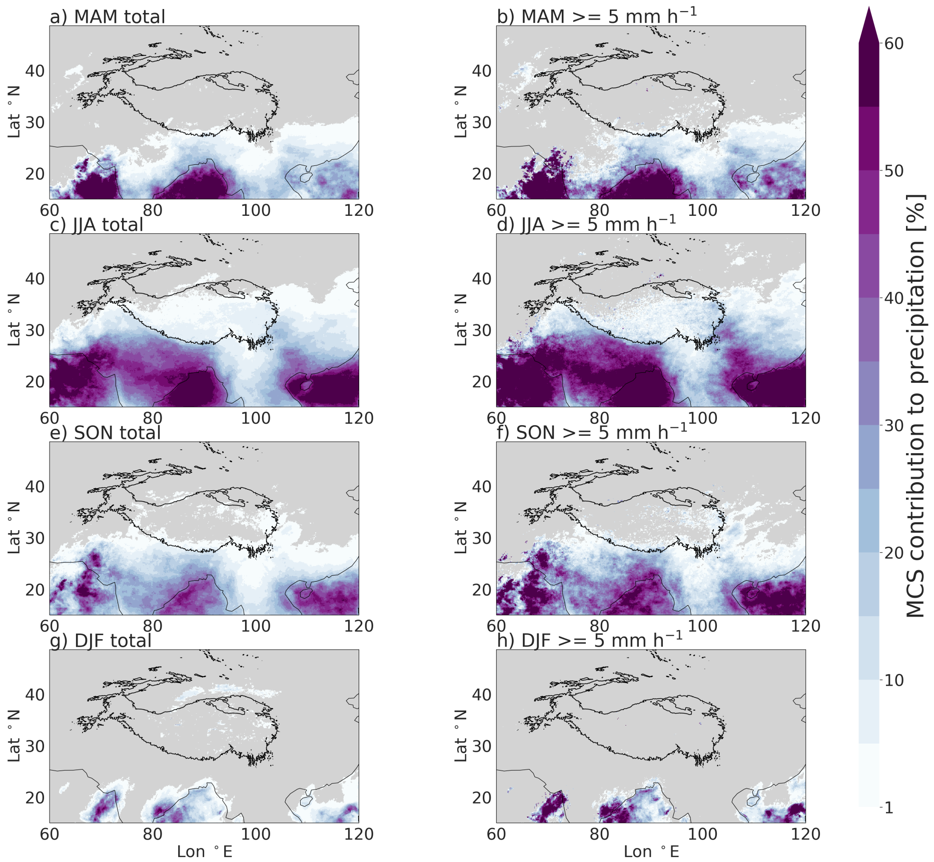

Figure 8. Maps of the seasonal contribution of precipitation from MCS [%] to the total precipitation (a,c,e,g) and to the total extreme precipitation, which is the sum of precipitation produced by rainfall of at least >=5 mm h^{-}1 (b,d,f,h).

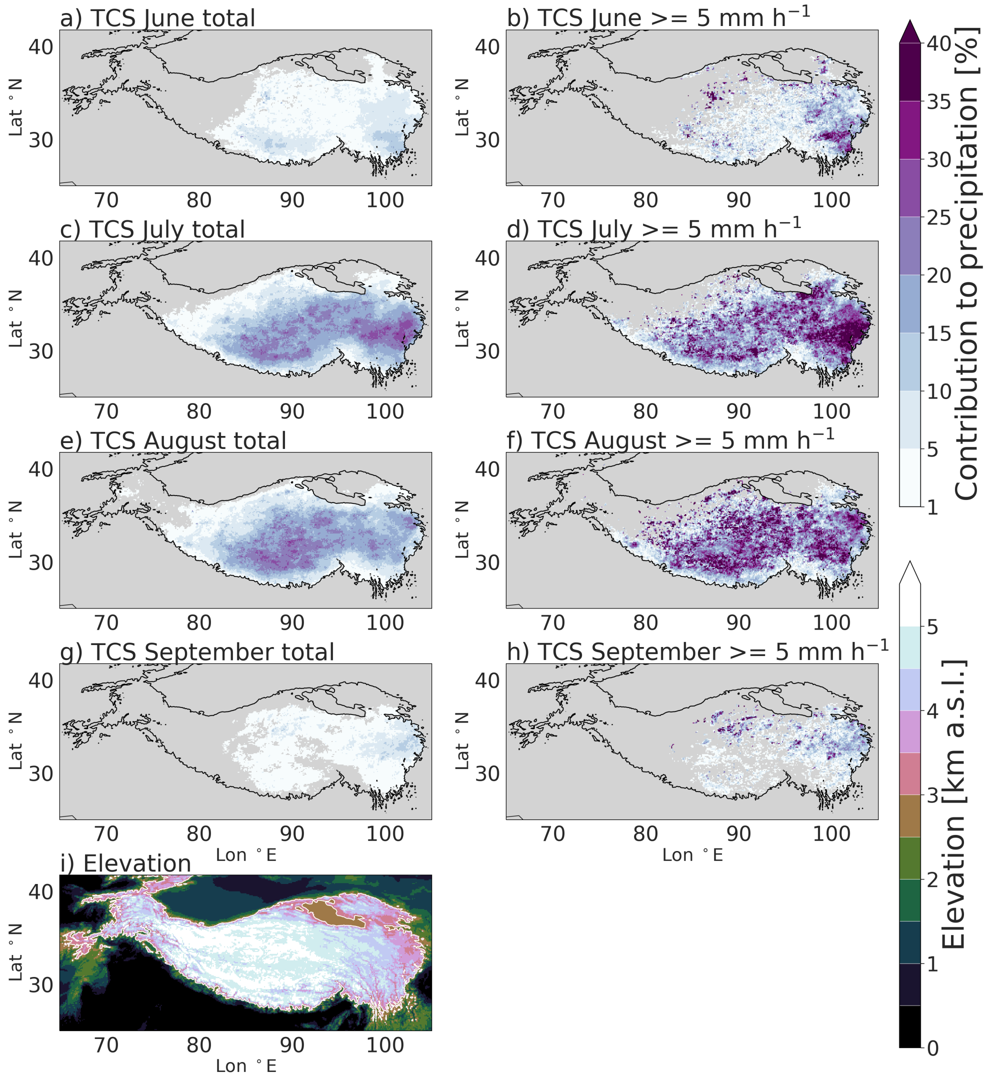

Figure 9. Maps of the contributions to total and total extreme precipitation from smaller and more short-lived convective cells over the TP (*TCS*) [%]. These convective cells have approximately meso-β dimensions in the horizontal plane (20 to 200 km). Contributions are shown for June to September as the ratio of precipitation from the convective cells to total precipitation (a,c,e,g) and to total extreme precipitation (b,d,f,h), defined as the sum of precipitation that fell at a rate of at least 5 mm h^{-}1. The elevation of the TP [km a.s.l.] is shown for context (i).

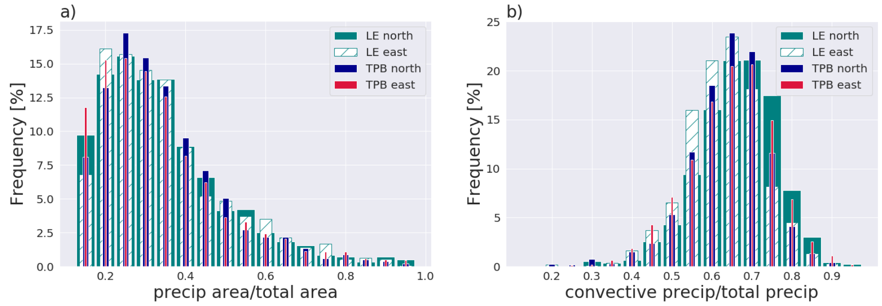

Figure 10. Histograms of a) the fraction of total cloud area that precipitates [precipitating area/total area] and b) the fraction of the precipitating cloud area associated with convective precipitation [convective precipitating/total precipitating area]. Convective precipitation is here defined as precipitation at a rate of at least 5 mm h−1.

part of an MCS produces large amounts of rainfall over short periods and is therefore of higher environmental and hydrological relevance than the stratiform part. The distribution of the precipitating area, expressed as a fraction of the total cloud area for all identified MCSs, is right-skewed, which shows that for more than half of the identified MCSs, only 10 % to 40 % of the detected cloud area produces precipitation (Fig. 10a). Only a small part of the entire cloud complex of an MCS produces precipitation, and the convective core usually covers an area even smaller than this. For more than 90 % of all identified and tracked MCSs, the histogram of the fraction of the precipitating area that corresponds to convective precipitation peaks between 0.6 and 0.8, which means that 60 % to 80 % of all precipitation from MCSs falls at rates of at least >= 5 mm h^{-1} (Fig. 10b). This is consistent with other studies, which have shown that around 40 % of precipitation in well-developed MCSs is stratiform, while around 60 % of the total rainfall is of convective type (Cheng & Houze, 1979; Rutledge & Houze Jr, 1987). LE north systems have generally larger convective contributions to total rainfall than the other three MCS types and TPB east systems have the smallest convective precipitation contributions (Fig. 10b).

Results from the different MCS tracking methods were similar, regardless of whether the cold core or the heavy rain core criterion was applied, as mentioned in section 2.2 (Table 1). This implies that MCS precipitation intensity is reflected in the observed brightness temperatures, with cooler temperatures corresponding to greater intensity. Figure 11) shows the average rain rates for the different MCS types as a function of the lowest brightness temperature threshold above which a contiguous area of at least 100 pixels exist. It is shown that MCS that have lower brightness temperatures also have higher average rain rates (Fig. 11). This suggests that more intense precipitation is produced by deeper cloud systems, which have higher cloud tops and therefore correspond to lower brightness temperature in IR images.

3.2.3 Heavy impact MCS

The total rainfall amount produced by an MCS depends on the system's lifetime, size and intensity. The four MCS types presented in Figure 5 include MCSs with highly variable track characteristics, and so we further divide each MCS type into three categories, according to lifetime, size and intensity (Fig. 12). To identify what characterizes an MCS with a large environmental impact, the different MCS classes are compared based on their total amount of convective precipitation they produce during their lifetime. Figure 12 shows the distributions of total convective precipitation for the three cat-

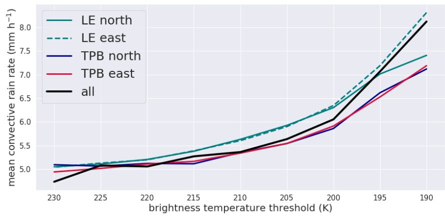

Figure 11. Mean convective rain rate [mm h^{-1}] as a function of the brightness temperature [K] for the coldest contiguous area in one MCS.

egories of lifetime, size and intensity for the MCS types LE north, LE east, TPB north and TPB east. The boxplot shows that the total amount of convective precipitation varies substantially between the tracked MCS. Differences between the total convective precipitation distributions for the four previously defined MCS types(LE north, LE east, TPB north, TPB east) are small, which supports our earlier finding that large-scale atmospheric systems, which determine MCS transport and genesis location, do not determine the environmental impact of the systems. Hence, both eastward- and northward-moving MCSs over lower and higher elevations, may produce substantial amounts of heavy rainfall. Comparing lifetime, area and intensity, for systems in the different categories, the most obvious difference is between systems that last longer than 24 hours and shorter-lived systems (Fig. 12a). The mean, maximum and outliers for the distributions of total convective precipitation all increase as the area covered by the system increases (Fig. 12b), and the total convective precipitation is not obviously related to the temperature of the convective part of the system (Fig. 12c).

MCSs which initiate over the TP (Fig. 3.1) are marked in red (Fig. 12) and are located in the lower-precipitation part of the distribution for each category. This means that systems which initiate over the TP produce little convective precipitation compared to those that form outside, or at the edges of the TP. The MCS observed on July 2008 (Fig. 3) is also marked in Figure 12 for context (red cross). This MCS persisted for 18 hours and produced more convective precipitation than most systems over the TP. It falls into the largest mean category, but produced less total convective precipitation than other systems which persisted for more than 24 hours (Fig. 12a-b).

The joint frequency distributions for total convective precipitation and maximum rain rate, system lifetime, maximum convective area and mean temperature of the lowest brightness temperature for a contiguous area (Fig. 13), show that lifetime and area have a greater effect on the environmental impact of the systems than rain rate intensity or brightness temperatures.

As stated earlier, MCSs may take different geometric shapes, ranging from elongated squall lines to quasi-circular MCCs. More elongated, or linear-shaped, systems have an eccentricity [minor axis/major axis] closer to 0, whereas more circular-shaped MCS have an eccentricity closer to 1. Figure 3.2.3a shows an example snapshot of a tracked MCS (August 17^{th}, 2012 at 13:30 UTC) with an eccentricity value of 0.77, which is typical value for an MCC (Maddox, 1980). As shown in Figure 3.2.3b, most systems tracked in the TP region have oval or ellipsoid shapes with eccentricity values between 0.3 and 0.6. We define MCSs with the highest environmental impact as those in the 90^{th} percentile of the total convective precipitation-distribution. These systems tend to be slightly more circular-shaped, relative to the eccentricity distribution that includes all tracked MCSs (Fig. 3.2.3b). Figure 3.2.3c,d shows the eccentricity distributions divided into the four subgroups LE north, LE east, TPB north and TPB east. All tracked systems in the

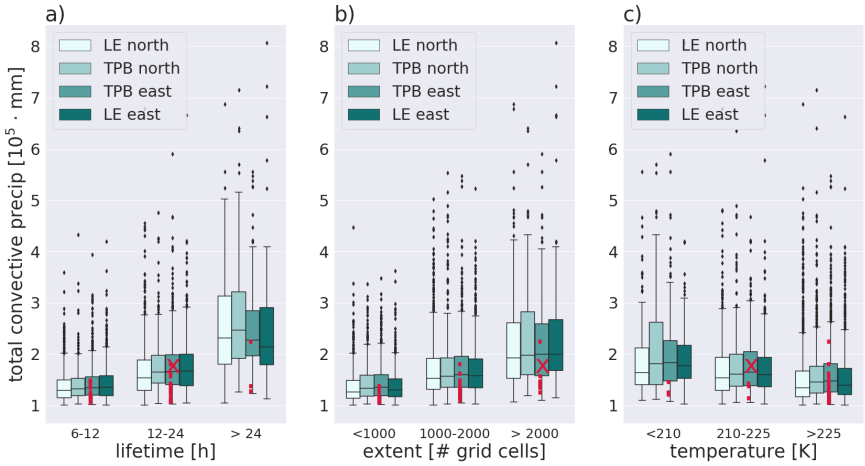

Figure 12. Boxplot showing the distribution of total convective precipitation produced by eastward- and northward-moving MCSs which cross the TP (TPB) and which remain in the surrounding lower-elevation plains (LE). MCSs are divided into different classes dependent on a) lifetime [h], b) extent [number of grid cells] and c) temperature [K]. The temperature refers to the lowest brightness temperature for a contiguous area within the cloud feature. The red dots show systems within the TPB group that remained over the TP and the red cross highlights the MCS from of July 2008 used as a case study (see section 2).

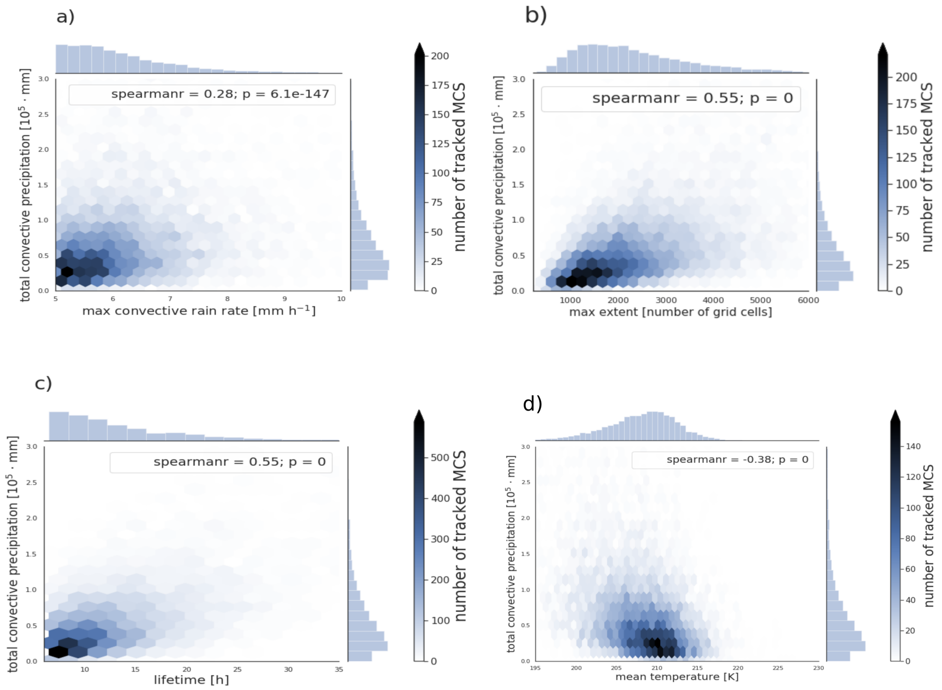

Figure 13. Frequency density plots for the total convective precipitation and a) maximum convective rain rate [mm h^{-1}], b) maximum convective area [number of grid cells] and c) lifetime [h] and d) mean brightness temperature [K] for all tracked MCS. The color scale reflects the number of identified MCS tracks which correspond to each part of the plotted space.

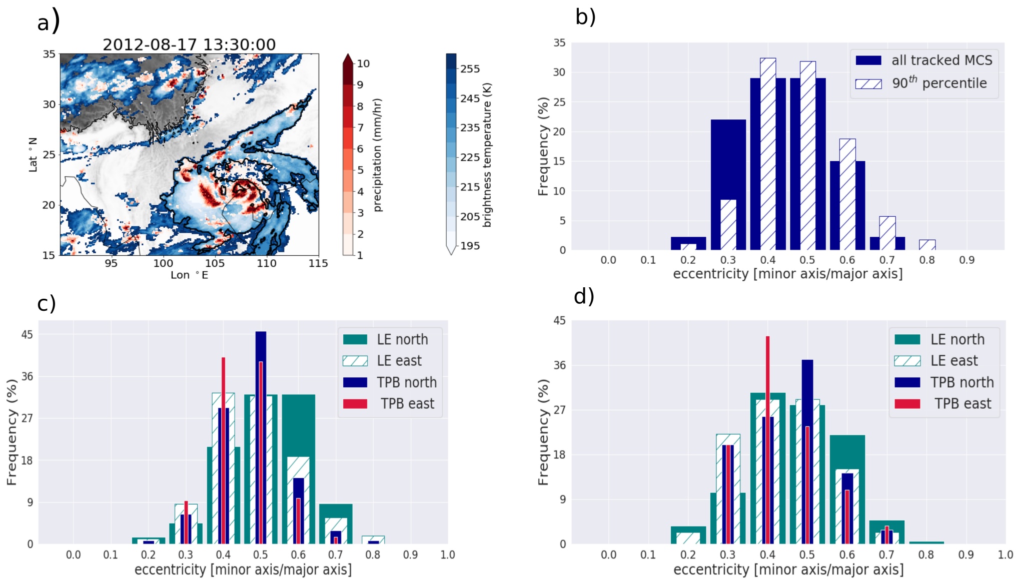

Figure 14. Eccentricity [minor axis length/major axis length] for tracked MCSs. a) An example of a quasi-circular MCS (August 17^{th}, 2012 at 13:30 UTC) with an eccentricity of 0.77, b) Histogram of eccentricity values for all tracked MCSs and for MCSs which produce the largest total amount of convective precipitation (rain rate of at least >=5 mm h^{hr}). These systems make up the 90^{th} percentile of the distribution of total convective precipitation; c) Histogram of eccentricity values for systems, divided into MCS classes: LE north, LE east, TPB north, TPB east; and d) same as c) but shown separately for MCS classes: LE north, LE east, TPB north, TPB east.

respective class are included in the distributions in (c), and the distributions in (d) include only systems that have the highest environmental impact, i.e. from the 90^th percentile of the total convective precipitation distribution for that class. It is clear that LE north and LE east systems are generally more circular-shaped than TPB east and TPB north systems (Fig. 3.2.3c), and MCSs with eccentricity greather than 0.5 become more frequent for heavy impact MCSs in the TPB east and TPB north classes (Fig. 3.2.3d). The figure shows that squall lines, which have a great environmental impact over the US Great Plains (Yang et al., 2017; Hitchcock et al., 2019), are not present in our study area. In contrast to the Great Plains in the USA, the most intense systems in our study area have slightly higher eccentricity values, particularly when the MCS is close to the TP, where the terrain most likely inhibits any quasi-linear organization of convection.

4 Discussion

4.1 Role of MCS for precipitation

Previous studies have highlighted the importance of MCS-induced precipitation as being the main source of summer precipitation over the TP. The reason for the discrepancy between that conclusion and our findings is most two-fold. Our method for MCS tracking is less likely to include cirrus clouds than more standard tracking methods, and our method for calculating MCS-associated precipitation differs from the commonly used methods. Many studies use a radius approach (L. Hu et al., 2017; Curio et al., 2019), where all precipitation within a certain radius of the MCS center is considered to be MCS-induced precipitation, instead of tracking precipitation features within cloud cells as we have done here. Our results show that the precipitating area of an MCS can vary significantly (Fig. 10), and the method we have used here therefore gives a more accurate estimation of precipitation associated with an MCS, relative to the size of the MCS. Moreover, we only track larger MCSs and exclude systems at the meso-β scale, which, as we could show, have higher contributions to summer precipitation over the TP.

This study shows that isolated, smaller-scale (m̃eso-β) convective cells make a greater contribution than MCSs (meso-α) to both seasonal mean precipitation and extreme summer precipitation, according to our tracking method. This result suggests that other convective modes, which are not captured by the applied tracking methods, are important and that topography and moisture conditions over the TP may inhibit the organization of convective cells into large systems. A similar conclusion was drawn by Houze et al. (2007) who investigated deep convective features based on Tropical Rainfall Measuring Mission (TRMM) Precipitation Radar (PR) data and found that deep convective echoes occur over the TP in a scattered manner, whereas more prominent mesoscale convective features organized along the Himalayan ranges. More complex convective modes (e.g. multi-cellular convective cells), which are not captured by the applied tracking, and convective cells with smaller horizontal extents are most likely more important for extreme precipitation. A possible explanation for the presence of isolated convective cells could be the occurrence of cirrus clouds at higher altitudes, which may locally inhibit convective heating during summer (Roebber et al., 2002). Satellite observations reveal a bimodal distribution of cloud top heights over the TP (D. Chen et al., 2018; Kukulies et al., 2019), whereby cloud top temperatures below 220 K correspond to cloud top heights above 10 km a.s.l. (D. Chen et al., 2018). The presence of isolated convective cells could therefore be an indicator of simultaneous occurrence of cirrus clouds and convective clouds.

However, occasionally larger MCSs according to the definition used here were also found over the TP (in total 58 cases). Most of the MCSs that formed over the TP were eastward-moving and resulted in heavy precipitation at the eastern edges of the TP. Although the amount of convective precipitation was relatively small compared to that from MCSs over the Indo-Gangetic Plain (due to generally lower intensity and lifetimes), these MCSs can be very destructive when they enter a populated downstream region and cause devastating floods, such occurred in July 2008 (X. Feng et al., 2014). More studies are needed to investigate future projections of both MCS intensity, but also MCS frequency over the TP and in the surrounding regions.

In the LE and in parts of the TPB region, the importance of MCSs for summer mean and extreme rainfall in summer was significantly higher than over the TP. Densely populated regions south of the Himalayas and in the Indo-Gangetic Plain experience frequent MCS events, which produce substantial rainfall amounts due to their longevity and large size. Z. Feng et al. (2018) found that long-lived MCS over the Great Plains in the USA produced 2–3 times more precipitation than short-lived MCSs. A similar result was found in this study, where both mean and maximum total convective precipitation of MCSs that persisted longer than 24 hours were twice as high as MCSs that persisted between 12 and 24 hours and thrice as high as MCS that persisted for up to 12 hours. The fact that there were no large differences in the contribution of precipitation from MCSs to the total seasonal and total extreme precipitation, shows that MCSs south of the TP are not only important for local extremes, but also important over climatological timescales. Changes in MCS patterns do not only affect the risk of severe weather for populated regions, but can also lead to changes in the hydrological cycle. It should be noted that the contribution of MCSs to precipitation may be underestimated for these regions in this study, because our MCS tracking method was optimized for the TP. Since cloud top temperatures for deep convective cells of the same depth are higher over lower-elevation regions than over regions at higher elevation, the differences between MCS-induced precipitation over the TP and in the LE region (such as the Indo-Gangetic Plain) may be even larger than is shown in our results.

To get a more complete understanding of the convective modes and their precipitation structure over the TP, further studies should consider the vertical aspects of the organization of convection. Radar observations of clouds over the southern Himalayas show mean radar reflectivities with convective signals over a height range between 3 and 14 km a.s.l. during summer (Kukulies et al., 2019). This may indicate MCSs in that region, but the temporal poor resolution of spaceborne radar observations means that there is a need for ground radar observations to confirm and investigate this.

4.2 Possible mechanisms for MCS formation

This study provides an observational perspective on MCSs over a region, where multiple processes may lead to the organization of convection at the mesoscale. Most of MCSs in the LE region over land were found south of the TP, over the Indo-Gangetic Plain and close to the Himalayas, as well as over the southern Indian subcontinent and the Bay of Bengal. Both land and ocean south of the TP are dominated by monsoon low pressure systems during the wet season, and these have been associated with barotropic instabilities and that may be amplified by wind-moisture feedbacks (Boos et al., 2017; Diaz & Boos, 2019). The results of this study show clearly that monsoon low pressure systems appear as large cloud clusters with similar dimensions as MCC ($\tilde{1}00\,000$ km^2).

The mechanisms for organization of convection over the TP are likely to be different because of the relatively limited moisture supply and the influence of local wind systems. The distinct diurnal evolution of MCSs (Fig. 3.1b), that are initiated over the TP and the large contributions of smaller-scale convective cells to precipitation suggest the importance of local conditions and topography. Surface properties, such as soil moisture have been suggested to be major contributing factor for MCS formation for the moist regions of the eastern TP (Sugimoto & Ueno, 2012). The systems that made the greatest convective contributions to precipitation over the TP in this study (including both MCSs and the smaller-scale convective cells) were also located in the east. The eastern TP is characterized by lower elevations and higher soil moisture, which may be crucial factors for the organization of convection. Outside of the monsoon season, when moisture supply to the TP is more limited, MCS could possibly form due to the lake-effect, which has been shown to trigger severe storms during winter (Dai et al., 2020).

While baroclinic instabilities are not among the the most important forcings for monsoon depressions (Diaz & Boos, 2019), upper-level baroclinicity has been found to be correlated with both different mesoscale disturbances over the TP, namely Tibetan Plateau vortices (TPV) (X. Feng et al., 2017; Curio et al., 2019), and Western disturbances (Hunt et al., 2018). This effect is mainly controlled by the strength and position of subtropical westerly jets when these systems form (Hunt et al., 2018). Mesoscale disturbances in relative vorticity occur frequently over the TP at around 500 hPa, particularly during the summer season (Curio et al., 2019). Thus, it should be noted that scattered precipitation features in satellite observations over the TP do not imply that mesoscale forcings are irrelevant for precipitation formation. This was demonstrated by Curio et al. (2019), who showed that a significant part of the plateau-scale precipitation occurs within a 3° radius of tracked Tibetan Plateau vortex centers. Even if these precipitation features do not occurred as contiguous areas of precipitation or embedded in contiguous cloud clusters, these may be still triggered by mesoscale disturbances. Studies into the linkages between TPVs and observations of MCSs and smaller-scale convective cells, could provide valuable valuable insights into mesoscale dynamics over the TP. Further, convection-permitting simulations could provide a more complete picture of the underlying dynamics for precipitation formation over the TP. In other regions, such as in North America, it could be shown that convection-permitting simulations realistically capture the main characteristics of MCSs and associated precipitation (Prein, Liu, Ikeda, Bullock, et al., 2017). So far, there are no studies that have looked at MCSs over the TP using model simulations with higher than 30 km-spatial resolution, although a few simulations with finer resolutions exist. The results from this study suggest that model simulations at higher resolutions are necessary for the effective representation of convective features over the TP region, particularly at elevations above 3000 m, where convective cells have much smaller spatial extents, relative to those over lower elevation surfaces. The existing and future fine resolution modeling over the TP should be used to explore the dynamics of the MCSs.

5 Summary and conclusions

This study provides an observational overview of mesoscale convective systems (MCS) in the Tibetan Plateau (TP) region and elucidates the role of MCSs for seasonal and extreme precipitation. We tracked MCSs by combining brightness temperatures from IR satellite imagery with the precipitation product GPM IMERG for the period 2000 to 2019. Spatial and temporal characteristics of MCS tracks and the structure of MCS-induced precipitation were examined for MCSs over the TP, MCSs that cross the TP boundary (TPB) and MCS over the surrounding lower-elevation plains (LE).

By comparing four different MCS tracking methods for the TP region, we have shown that it is useful to apply an additional criterion for more accurate MCS identification. To be considered an MCS, a cloud feature must contain either a region below 200 K (T_b cold core) or a region with rain rates equal to or above 5 mm h^{-1} that extends over at least ten grid cells (T_b heavy rain core). This reduces the number of falsely identified MCSs due to the presence of cirrus clouds or cold surfaces in higher mountain regions, resulting in a more realistic seasonal cycle for MCS frequency with a summer peak. There is a strong relationship between low brightness temperatures and heavy precipitation, and the T_b cold core and T_b heavy rain core criteria therefore resulted in identification of almost the same number of MCS tracks and similar MCS characteristics. This implies that these criteria can be used interchangeably, but the use of both precipitation and brightness temperature remains advantageous because it allows precipitation features to be identified and examined in the tracked clouds cells.

Most of the MCSs identified using our MCS tracking method were found over the Indian subcontinent and Bay of Bengal. Major regions of genesis for MCSs that crossed the TPB were the Indo-Gangetic Plain and the south of the Himalayan mountain range. In these regions, MCSs account between 10 % and 55 % of total precipitation between July and August and between 10 % and 70 % to total extreme precipitation in summer. A large part of the tracked MCS in the study area are characterized by quasi-circular cloud cells with large areas that are comparable to Mesoscale Convective Clusters (MCC). Further, MCS which produced the highest total convective precipitation amounts were characterized by longevity and large cloud extents rather than by high intensities.

MCSs over the TP were less frequent and represented only a small subgroup of MCSs identified at the TPB. We have shown that the contribution of MCS-induced precipitation to the total summer precipitation (total summer extreme precipitation) was only 1 % to 10 % (1 % to 30 %), which is significantly smaller than has been found in previous studies and is lower than for the surrounding regions. Additionally, the total amount of convective precipitation produced by MCS over the TP was also smaller compared to its surroundings, since MCS over the TP were generally smaller and more short-lived. In contrast, the results of tracking smaller-scale (m̃eso-β scale) and more short-lived convective cells showed that these made significantly higher contributions to the total and the total extreme precipitation over the TP in July and August. This result highlights the significance of more localized precipitation systems and convective modes to total summer precipitation over the TP. Many studies focus on frequently occurring mesoscale vorticity disturbances over the TP, for example Tibetan Plateau vortices (TPV) and Western Disturbances, and the results from this study suggest that there is a more complex relationship between mesoscale dynamics and the scattered and isolated precipitation and cloud features identifiable in observations. Model simulations at convective scales could help to improve the understanding of mesoscale dynamics for precipitation formation over the TP.

Acknowledgments

The study was supported by the Swedish National Space Agency (SNSA: 188/18 4) and the Chinese Academy of Sciences (XDA2006040103). This is a contribution no XXX to CORDEX-FPS-CPTP. We thank the providers of key data sets used here (NASA, NCEP). NCEP/CPC Brightness temperatures can be downloaded from `https://disc.gsfc.nasa.gov/datasets/GPM\_MERGIR\_V1/summary` and GPM IMERG can be downloaded from `https://disc.gsfc.nasa.gov/datasets/GPM_3IMERGHH_06/summary?keywords=GPM\%20IMERG\%20v06\%2030\%20MIN`. The code for the MCS tracking algorithm can be found at `https://github.com/JuliaKukulies/mcs_tracking/tree/master/CTT/tracking`.

References

Ban, N., Schmidli, J., & Schär, C. (2015). Heavy precipitation in a changing climate: Does short-term summer precipitation increase faster? *Geophysical Research Letters*, *42*(4), 1165–1172.

Berg, P., Moseley, C., & Haerter, J. O. (2013). Strong increase in convective precipitation in response to higher temperatures. *Nature Geoscience*, *6*(3), 181–185.

Bibi, S., Wang, L., Li, X., Zhou, J., Chen, D., & Yao, T. (2018). Climatic and associated cryospheric, biospheric, and hydrological changes on the tibetan plateau: a review. *International Journal of Climatology*, *38*, e1–e17.

Boos, W. R., Mapes, B. E., & Murthy, V. S. (2017). Potential vorticity structure and propagation mechanism of indian monsoon depressions. In *The global monsoon system: Research and forecast* (pp. 187–199). World Scientific.

Cheeks, S. M., Fueglistaler, S., & Garner, S. T. (2020). A satellite-based climatology of central and southeastern us mesoscale convective systems. *Monthly Weather Review*, *148*(6), 2607–2621.

Chen, D., Guo, J., Wang, H., Li, J., Min, M., Zhao, W., & Yao, D. (2018). The cloud top distribution and diurnal variation of clouds over east asia: Preliminary results from advanced himawari imager. *Journal of Geophysical Research: Atmospheres*, *123*(7), 3724–3739.

Chen, G., & Kirtman, B. P. (2018). Long-lived mesoscale convective systems of superparameterized cam and the response of cam. *Journal of Advances in Modeling Earth Systems*, *10*(9), 2269–2286.

Cheng, C.-P., & Houze, R. A. (1979). The distribution of convective and mesoscale precipitation in gate radar echo patterns. *Monthly Weather Review*, *107*(10), 1370–1381.

Curio, J., Schiemann, R., Hodges, K. I., & Turner, A. G. (2019). Climatology of tibetan plateau vortices in reanalysis data and a high-resolution global climate model. *Journal of Climate*, *32*(6), 1933–1950.

Dai, Y., Chen, D., Yao, T., & Wang, L. (2020). Large lakes over the tibetan plateau may boost snow downwind: implications for snow disaster. *Science Bulletin*.

Diaz, M., & Boos, W. R. (2019). Barotropic growth of monsoon depressions. *Quarterly Journal of the Royal Meteorological Society*, *145*(719), 824–844.

Esmaili, R. B., Tian, Y., Vila, D. A., & Kim, K.-M. (2016). A lagrangian analysis of cold cloud clusters and their life cycles with satellite observations. *Journal of Geophysical Research: Atmospheres*, *121*(19), 11–723.

Feidas, H. (2017). Satellite-observed features of a mesoscale convective complex over se europe. *International Journal of Remote Sensing*, *38*(22), 6219–6246.

Feng, X., Liu, C., Fan, G., & Zhang, J. (2017). Analysis of the structure of different tibetan plateau vortex types. *Journal of Meteorological Research*, *31*(3), 514–529.

Feng, X., Liu, C., Rasmussen, R., & Fan, G. (2014). A 10-yr climatology of tibetan plateau vortices with ncep climate forecast system reanalysis. *Journal of Applied Meteorology and Climatology*, *53*(1), 34–46.

Feng, Z., Leung, L. R., Houze Jr, R. A., Hagos, S., Hardin, J., Yang, Q., ... Fan, J. (2018). Structure and evolution of mesoscale convective systems: Sensitivity to cloud microphysics in convection-permitting simulations over the united states. *Journal of Advances in Modeling Earth Systems*, *10*(7), 1470–1494.

Fitzpatrick, R. G., Parker, D. J., Marsham, J. H., Rowell, D. P., Guichard, F. M., Taylor, C. M., ... others (2020). What drives the intensification of mesoscale convective systems over the west african sahel under climate change? *Journal of Climate*, *33*(8), 3151–3172.

Flohn, H., & Reiter, E. R. (1968). Contributions to a meteorology of the tibetan highlands. *Atmospheric science paper; no. 130*.

Fritsch, J., Kane, R., & Chelius, C. (1986). The contribution of mesoscale convective weather systems to the warm-season precipitation in the united states. *Journal of climate and applied meteorology*, *25*(10), 1333–1345.

Gaál, L., Molnar, P., & Szolgay, J. (2014). Selection of intense rainfall events based on intensity thresholds and lightning data in switzerland. *Hydrology and Earth System Sciences*, *18*(5), 1561–1573.

Guo, Z.-y., Dai, X.-y., Wu, J.-p., & Lin, H. (2006). Analysis of mesoscale convective systems over tibetan plateau in summer. *Chinese Geographical Science*, *16*(2), 116–121.

Heikenfeld, M., Marinescu, P. J., Christensen, M., Watson-Parris, D., Senf, F., Van Den Heever, S. C., & Stier, P. (2019). tobac v1. 0: towards a flexible framework for tracking and analysis of clouds in diverse datasets. *Geoscientific Model Development Discussions*.

Hitchcock, S. M., Schumacher, R. S., Herman, G. R., Coniglio, M. C., Parker, M. D., & Ziegler, C. L. (2019). Evolution of pre-and postconvective environmental profiles from mesoscale convective systems during pecan. *Monthly Weather Review*, *147*(7), 2329–2354.

Houze, R. A. (2004). Mesoscale convective systems. *Reviews of Geophysics*, *42*(4).

Houze, R. A., Wilton, D. C., & Smull, B. F. (2007). Monsoon convection in the himalayan region as seen by the trmm precipitation radar. *Quarterly Journal of the Royal Meteorological Society: A journal of the atmospheric sciences, applied meteorology and physical oceanography*, *133*(627), 1389–1411.

Hu, H., Leung, L. R., & Feng, Z. (2020). Observed warm-season characteristics of mcs and non-mcs rainfall and their recent changes in the central united states. *Geophysical Research Letters*, *47*(6), e2019GL086783.

Hu, L., Deng, D., Xu, X., & Zhao, P. (2017). The regional differences of tibetan convective systems in boreal summer. *Journal of Geophysical Research: Atmospheres*, *122*(14), 7289–7299.

Hunt, K., Curio, J., Turner, A., & Schiemann, R. (2018). Subtropical westerly jet influence on occurrence of western disturbances and tibetan plateau vortices. *Geophysical Research Letters*, *45*(16), 8629–8636.

Hurley, J. V., & Boos, W. R. (2015). A global climatology of monsoon low-pressure systems. *Quarterly Journal of the Royal Meteorological Society*, *141*(689), 1049–1064.

Jiang, J.-x., & Fan, M.-z. (2002). Convective clouds and mesoscale convective systems over the tibetan plateau in summer. *Chin. J. Atmos. Sci*, *26*(2), 263–270.

Klein, C., Belušić, D., & Taylor, C. M. (2018). Wavelet scale analysis of mesoscale convective systems for detecting deep convection from infrared imagery. *Journal of Geophysical Research: Atmospheres*, *123*(6), 3035–3050.

Kukulies, J., Chen, D., & Wang, M. (2019). Temporal and spatial variations of convection and precipitation over the tibetan plateau based on recent satellite observations. part i: Cloud climatology derived from cloudsat and calipso. *International Journal of Climatology*, *39*(14), 5396–5412.

Kukulies, J., Chen, D., & Wang, M. (2020). Temporal and spatial variations of convection, clouds and precipitation over the tibetan plateau from recent satellite observations. part ii: Precipitation climatology derived from global precipitation measurement mission. *International Journal of Climatology*.

Li, Y., Yun, W., Yang, S., Liang, H., Shouting, G., & Fu, R. (2008). Characteristics of summer convective systems initiated over the tibetan plateau. part i: Origin, track, development, and precipitation. *Journal of applied meteorology and climatology*, *47*(10), 2679–2695.

Maddox, R. A. (1980). Mesoscale convective complexes. *Bulletin of the American Meteorological Society*, 1374–1387.

Morel, C., & Senesi, S. (2002). A climatology of mesoscale convective systems over europe using satellite infrared imagery. ii: Characteristics of european mesoscale convective systems. *Quarterly Journal of the Royal Meteorological Society: A journal of the atmospheric sciences, applied meteorology and physical oceanography*, *128*(584), 1973–1995.

Orlanski, I. (1975). A rational subdivision of scales for atmospheric processes. *Bulletin of the American Meteorological Society*, 527–530.

Prein, A. F., Liu, C., Ikeda, K., Bullock, R., Rasmussen, R. M., Holland, G. J., & Clark, M. (2017). Simulating north american mesoscale convective systems with a convection-permitting climate model. *Climate Dynamics*, 1–16.

Prein, A. F., Liu, C., Ikeda, K., Trier, S. B., Rasmussen, R. M., Holland, G. J., & Clark, M. P. (2017). Increased rainfall volume from future convective storms in the us. *Nature Climate Change*, *7*(12), 880–884.

Rasmussen, K. L., & Houze Jr, R. A. (2012). A flash-flooding storm at the steep edge of high terrain: disaster in the himalayas. *Bulletin of the American Meteorological Society*, *93*(11), 1713–1724.

Redelsperger, J.-L., Diongue, A., Diedhiou, A., Ceron, J.-P., Diop, M., Gueremy, J.-F., & Lafore, J.-P. (2002). Multi-scale description of a sahelian synoptic weather system representative of the west african monsoon. *Quarterly Journal of the Royal Meteorological Society: A journal of the atmospheric sciences, applied meteorology and physical oceanography*, *128*(582), 1229–1257.

Roebber, P. J., Schultz, D. M., & Romero, R. (2002). Synoptic regulation of the 3 may 1999 tornado outbreak. *Weather and Forecasting*, *17*(3), 399–429.

Romatschke, U., Medina, S., & Houze Jr, R. A. (2010). Regional, seasonal, and diurnal variations of extreme convection in the south asian region. *Journal of climate*, *23*(2), 419–439.

Rossow, W. B., & Schiffer, R. A. (1999). Advances in understanding clouds from isccp. *Bulletin of the American Meteorological Society*, *80*(11), 2261–2288.

Rutledge, S. A., & Houze Jr, R. A. (1987). A diagnostic modelling study of the trailing stratiform region of a midlatitude squall line. *Journal of the atmospheric sciences*, *44*(18), 2640–2656.

Schädlich, S., Göttsche, F., & Olesen, F.-S. (2001). Influence of land surface parameters and atmosphere on meteosat brightness temperatures and generation of land surface temperature maps by temporally and spatially interpolating atmospheric correction. *Remote Sensing of Environment*, *75*(1), 39–46.

Shi, X., Wang, Y., & Xu, X. (2008). Effect of mesoscale topography over the tibetan plateau on summer precipitation in china: A regional model study. *Geophysical Research Letters*, *35*(19).

Sugimoto, S., & Ueno, K. (2012). Role of mesoscale convective systems developed around the eastern tibetan plateau in the eastward expansion of an upper tropospheric high during the monsoon season. *Journal of the Meteorological Society of Japan. Ser. II*, *90*(2), 297–310.

Tao, S.-y., & Ding, Y.-h. (1981). Observational evidence of the influence of the qinghai-xizang (tibet) plateau on the occurrence of heavy rain and severe convective storms in china. *Bulletin of the American Meteorological Society*, *62*(1), 23–30.

Vondou, D. A., Nzeukou, A., & Kamga, F. M. (2010). Diurnal cycle of convective activity over the west of central africa based on meteosat images. *International journal of applied earth observation and geoinformation*, *12*, S58–S62.

Wang, B. (1987). The development mechanism for tibetan plateau warm vortices. *Journal of the atmospheric sciences*, *44*(20), 2978–2994.

Wang, C., Luo, J., Rossow, W. B., & Pearl, C. (2018). Production of globally uniform isccp convection tracking (ct) dataset and preliminary analysis results. *AGUFM*, *2018*, A11J–2361.

Xiang, S., Li, Y., Li, D., & Yang, S. (2013). An analysis of heavy precipitation caused by a retracing plateau vortex based on trmm data. *Meteorology and Atmospheric Physics*, *122*(1-2), 33–45.

Yang, Q., Houze Jr, R. A., Leung, L. R., & Feng, Z. (2017). Environments of long-lived mesoscale convective systems over the central united states in convection permitting climate simulations. *Journal of Geophysical Research: Atmospheres*, *122*(24), 13–288.

Yao, T., Xue, Y., Chen, D., Chen, F., Thompson, L., Cui, P., . . . others (2019). Recent third pole's rapid warming accompanies cryospheric melt and water cycle intensification and interactions between monsoon and environment: Multidisciplinary approach with observations, modeling, and analysis. *Bulletin of the American Meteorological Society*, *100*(3), 423–444.

Yasunari, T., & Miwa, T. (2006). Convective cloud systems over the tibetan plateau and their impact on meso-scale disturbances in the meiyu/baiu frontal zone. *Journal of the Meteorological Society of Japan. Ser. II*, *84*(4), 783–803.

Ye, D.-Z., & Wu, G.-X. (1998). The role of the heat source of the tibetan plateau in the general circulation. *Meteorology and Atmospheric Physics*, *67*(1-4), 181–198.

Yuan, J., & Houze Jr, R. A. (2010). Global variability of mesoscale convective system anvil structure from a-train satellite data. *Journal of Climate*, *23*(21), 5864–5888.

Zhang, L., Su, F., Yang, D., Hao, Z., & Tong, K. (2013). Discharge regime and simulation for the upstream of major rivers over tibetan plateau. *Journal of Geophysical Research: Atmospheres*, *118*(15), 8500–8518.